FAR-FIELD NANOSCALE THERMAL AND STRUCTURE IMAGING

N301

Xiaoduan Tang, Shen Xu, Xinwei Wang

[1] Department of Mechanical Engineering, Iowa State University, Ames, Iowa, 50011, USA

Abstract

The imaging resolution of a conventional optical microscope is limited by diffraction to about half of the illuminating wavelength. A micro/submicron particle induced near-field effect can focus an incident laser beam to a small region of tens of nanometres. Using self-assembled transparent microspheres as far-field superlenses (FSLs), here we report the first experimental demonstration of combined structural, thermal, and stress imaging at a 20 nm resolution ($< \lambda/26$, $\lambda = 532$ nm), even though the laser beam is at μm size. FSLs are integrated into a confocal Raman spectrometer and microscope system to overcome the diffraction limit. Periodical surface structure, thermal and stress information is examined. Furthermore, electromagnetic simulation is conducted to well interpret the experimental results. FSLs provide new opportunities in nanoscale imaging, nanolithography and nanotexturing.

Introduction

The conventional optical microscope is diffraction-limited in imaging resolution to about half of the illuminating wavelengths. Near-field scanning optical microscopy (NSOM) is capable of breaking the optical resolution limit by extensively employing the properties of evanescent waves [1]. Stochastic optical reconstruction microscopy (STORM) provided a high imaging resolution of approximately 20 nm by controlling the fluorescence emission from a single molecule [2]. Whereas these techniques are nearsighted, FSLs capable of imaging beyond the diffraction limit in the far field were developed. A FSL used optically transparent microspheres to overcome the white-light diffraction limit with a resolution between $\lambda/8$ and $\lambda/14$ [3]. Regarding nanoscale surface thermal imaging, scanning thermal microscope (SThM) has been reported as an established technique to measure nanoscale temperature distributions with a spatial resolution of ~50 nm [4].

Monolayer of nanoparticles is attractive due to the generation of surface textures. Laser-assisted nanopatterning and nanoimprinting lithography has been proved to be able to pattern nanoscale features on substrates [5]. Due to the wide application of particles, theoretical studies about optical and temperature field enhancements by particles have been conducted [6]. Nanoscale experimental imaging using microparticles is rarely reported, however. McLeod and Arnold employed a microsphere as an objective lens for nanopatterning by focusing a laser beam on a substrate [5]. Arbitrary patterns and individual features were generated with a minimum size of 100 nm. Wang *et al.* employed transparent microspheres to collect near-field object information and formed virtual images at a 50 nm resolution [3]. In this work, a combined far-field nanoscale thermal, stress and structure imaging of silica particles on a silicon substrate under laser irradiation is conducted for the first time using Raman spectroscopy at a 20 nm lateral resolution. The electromagnetic field inside the substrate-particle system is simulated to interpret the measurement results.

Experimental Details

Sample Preparation

The tilting technique is employed to pattern silica particles in a monolayer on silicon wafers [7]. Surfactant (triton-X: methanol = 1:400 by volume) is mixed with monodisperse silica particle suspensions. The suspensions have silica particles with a solid percentage of 10 % suspended in water. Silica spheres of 200 nm (Corpuscular, Inc.), 400 nm (Polysciences, Inc.), 800 nm, and 1210 nm (Bangs Laboratories, Inc.) diameters are used without any surface treatment. Silicon (100) wafers (University Wafer) are cleaned in acetone and then deionized water for an hour with ultrasonic agitation. These wafers are placed on glass slides, which are tilted on a table with an angle of about 10° [7]. The mixture is dispensed onto substrates using a syringe and left to dry for about half an hour in the air. Then a 2-D monolayer of particles is formed on the substrate. Figure 1 shows typical scanning electron microscope (SEM) images of silica monolayers of 1210 nm diameter assembled on silicon wafers. The average diameter of the particles is about 1120 nm, a little smaller than the nominal diameter.

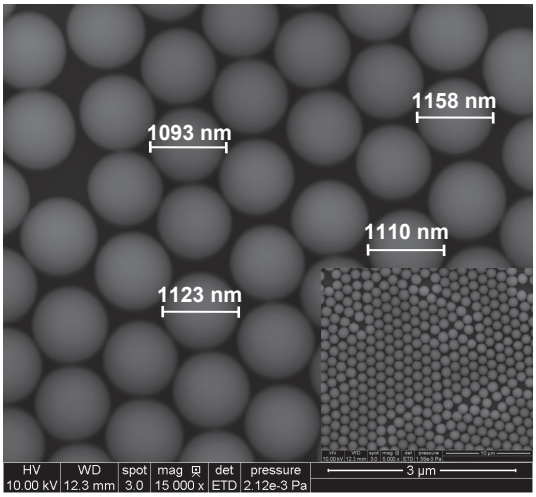

Figure 1. SEM images of two-dimentional monolayer array of silica particles assembled on a silicon wafer.

Experimental Method

Figure 2(a) shows schematic of the experimental setup. The Raman scattering system consists of a confocal Raman spectrometer (Voyage^{TM}, B&W Tek) and a microscope (Olympus BX51). Raman spectra are taken at room temperature by using a 532 nm laser line. The laser beam is focused by an objective lens. A sample is placed on a 3-D piezo-actuated nano-stage (ThorLabs MAX312). The travel range of the 3-D nano-stage is 20 µm in each direction, with a resolution of 20 nm. The incident laser used as both Raman probing and heating source is focused by the objective lens on the silica particles at first. Due to the effect of particle, the laser beam is further focused on the silicon substrate and heats up the substrate. The excited Raman scattering signal and Rayleigh scattering signal are collected through the same objective. A group of Raman spectra are obtained before imaging measurement in order to determine the focal level in the z direction. The sample is then fixed at the laser focal spot without any vertical shift. The temperature rise inside the substrate achieves the highest value at the focal spot. Environmental factors such as the change of room temperature and movement of the objective will lead to Raman spectra differences. Therefore, the imaging process is followed immediately to minimize the effect of environmental factors. The sample is scanned along the x direction with a step of 27 or 53 nm in a range from 0.5 to 4.0 µm (Figure 2(b)). The movement is controlled electrically without any touch of the sample, stage, Raman spectrometer, microscope and other related equipment that would affect the quality of Raman signal. The Raman spectra changing with the nanoscale movement of the sample is finally obtained.

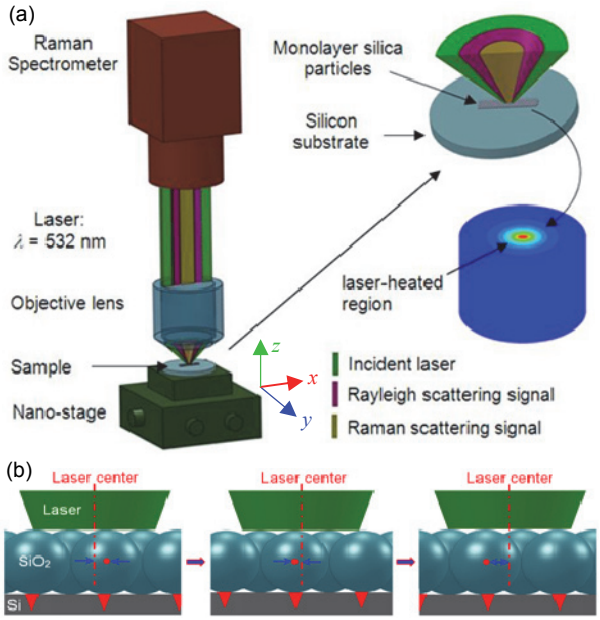

Figure 2. (a) Schematic of the experimental setup (not to scale). (b) Movements of sample relative to the incident laser in the x direction.

Temperature and Stress Dependence of Raman Scattering in Silicon

In order to determine the thermal and stress response inside silicon substrate under laser irradiation, the temperature dependence of Raman shift and full wave at half maximum (FWHM) and stress dependence of Raman shift are needed. Balkanski *et al.* presented two theoretical models of Raman frequency and FWHM changing with temperature from 5 to 1400 K [8]. The models show that both relationships are linear within a temperature range from 300 - 600 K. The linear fitting slope of Raman shift against temperature reported in literature is -0.022 cm^{-1}/K [9]. For Raman FWHM against temperature, the slope is 0.01 cm^{-1}/K [10]. In our calibration, the obtained fitting slope for the Raman shift against temperature is -0.022 cm^{-1}/K and the slope for the Raman FWHM versus temperature is 0.0082 cm^{-1}/K in temperatures from 300 - 440 K, which agree well with the literature values. A theoretical relation between the shift of Raman frequency and the uniaxial stress inside silicon has been developed [11]. The Raman frequency varies linearly with the in-plane stress with a proportionality constant of -3.6 cm^{-1}/GPa [9]. The Raman FWHM is little influenced by thermal stress. The combined use of Raman shift and FWHM determines the temperature rise inside the laser-heated sample and the thermal stress induced by the temperature gradient.

Thermal Probing of Silicon Under Silica Particles

In the experiments, the focal level, particle size and laser energy are important factors for determining the near-field heating. In order to investigate the near-field heating effect caused by laser irradiation, Raman scattering is performed with four laser powers of 2.0, 3.0, 5.5 and 6.9 mW, corresponding to energy fluxes of 2.5×10^8, 3.8×10^8, 6.9×10^8 and 8.6×10^8 W/m^2, respectively.

During the experiments, the group for silica particles with diameter of 1210 nm under laser energy flux of 8.6×10^8 W/m^2 is first conducted. Two groups of Raman spectra for bare silicon and silicon with 1210 nm diameter silica particles on the top are obtained, with integration time of 1 s. The Raman FWHMs for bare silicon and silicon with particles are 6.31 cm^{-1} and 6.77 cm^{-1}, respectively. It indicates a temperature rise of 55.8 K based on the broadening of Raman FWHM (0.46 cm^{-1}). Using the Raman shift information, the Raman shift difference (0.64 cm^{-1}) between bare silicon and silicon with particles gives a temperature rise of 29.3 K. As shown in Figure 3, the temperature rises assessed based on the Raman shift are lower than those based on the Raman FWHM method. The differences between the two methods are mainly due to the temperature gradient and compressive stress around the laser-heated spot [9, 10]. As the temperature increases, the number of phonons rises and the lifetime decreases. The increase of Raman FWHM indicates the temperature rise inside silicon, as FWHM is little influenced by thermal stress. The Raman shift is affected by both temperature difference and thermal stress. The laser beam heats up the sample within an extremely focusing area. The heated area tends to expand and raise pressure to the nearby cold silicon substrate. The local pressure causes a distortion of the crystal lattice and the equilibrium positions of the atoms are changed, which causes lattice variation. An additional shift is added in Raman frequency due to the stress besides temperature rise. The stress effect induced by particle-focused laser heating drags the Raman peak to the higher wavenumber (lower temperature) direction. Therefore, the temperature rise obtained based on the Raman shift method is lower than that based on the Raman FWHM method. The combined use of these two methods gives comprehensive understanding of how high the sample can be heated up and whether there exists any thermal stress.

The same experimental method is employed to measure the temperature rise for the situation of silica particles with 1210 nm diameter under three other laser energy fluxes of 2.5×10^8, 3.8×10^8, and 6.9×10^8 W/m^2. All the experimental procedures for silica particles with 800 and 400 nm diameters under four different laser energy fluxes are the same with that of 1210 nm particles. Figure 3 shows the relationship between temperature rise of silicon and diameter of silica particles. With the increase of particle size, the incident laser is more focused on the silicon substrate, and the temperature rise is higher. Under energy flux of 8.6×10^8 W/m^2, the temperature rise is 11.1 K for silica particles of 400 nm diameter, 16.2 K for those of 800 nm, and 55.8 K for those of 1210 nm, according to the Raman FWHM method. As the particle size increases from 400 to 800 nm, the temperature rise increases by about 45%. When the particle size increases to 1210 nm, the temperature rise goes up to 5 times that for 400 nm particles. Similar trends for temperature rise can be found in the results for other laser energy fluxes. All the curves conclude that the temperature rise increases exponentially with silica particle diameter in the range from 400 to 1210 nm.

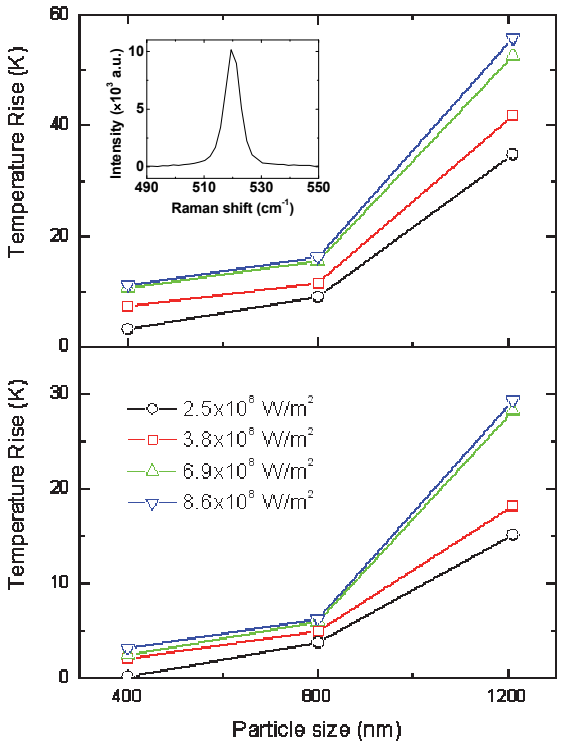

Figure 3. The relationship between temperature rise in silicon against diameter of silica particle. The upper figure shows the temperature rise assessed based on the Raman FWHM, and the lower figure is based on the Raman shift method. The differences are due to the thermal stress. The inset figure shows a typical Raman spectrum of silicon.

Nanoscale Imaging of Self-assembled Particles

Four groups of Raman spectra for silicon beneath particles are obtained for the 1210-nm-particle case under laser irradiation of different energy fluxes. The sample is moved relative to the laser along the x direction (see Figure 2) in a range of 4.0 μm with a step of 53 nm. The Raman intensity increases linearly with the energy flux. The highest Raman intensities (I_{max}s) are 1.30×10^4, 2.08×10^4, 3.83×10^4 and 4.67×10^4 for energy fluxes of 1.2×10^9, 2.0×10^9, 3.7×10^9 and 4.7×10^9 W/m^2, respectively. As the variation trends of the temperature and stress are the same for different energy fluxes, here we only analyse the case for 3.7×10^9 W/m^2. Other cases can be treated similarly. The Raman intensity I, frequency ω and FWHM Γ of silicon vary periodically along the x direction and are shown in Figure 4. About three periods are found within the travel range in the figure. The period length decreases from left to right. The difference may due to the diameter difference, the interspace among particles, and the backlash of the stage. For the first 3/4 period, half of the period length is 906 nm, much longer than the average particle radius (560 nm). For the second and third period, the period lengths are 1226 and 1013 nm, respectively, close to the average particle diameter (1120 nm). In the second period, the intensity difference between I_{max} and I_{min} is 2.37×10^4, with an intensity ratio (I_{max}/I_{min}) of 2.58. 1/64 of the period length is about 19 nm (as shown in the figure) with an intensity difference and ratio of about 2800 and 1.12, respectively. This difference can be distinguished at this scale in our experiment. As the intensity is the raw datum without any further processing, it is the best quality to specify the resolution. It is conclusive that the imaging resolution can be down to 20 nm.

Raman frequency ω changes in a range from 518.2 - 519.8 cm^{-1}, with a maximum shift of 1.6 cm^{-1}. FWHM Γ changes from 6.0 to 7.7 cm^{-1}, with a maximum difference of 1.7 cm^{-1}. In one period, ω increases from the lowest to highest value with a distance of 853 nm, and then decreases in a range of 320 nm. The variation of Γ is contrary to ω. It first decreases and then increases. The increasing and decreasing distances for both ω and Γ are of 533 nm difference. There are three main reasons that can account for the difference. First, the laser beam is continuously heating the sample during the experiments, and the integration time is very short. The heat produced by the laser at one step may affect the temperature field of the next step as the experimental process continues. Therefore, the high temperature decreasing distance is longer than the temperature increasing process. Second, as the laser may propagate with a small angle to the normal direction, there is a transverse distance between the focusing point inside silicon and the particle centre. When the sample moves relative to the oblique laser, the variations of the ω and Γ curves are not symmetric. Third, a part of the Raman signal came from the silicon wafer under the spacing among particles. As the laser beam was pre-focused on the particles by the objective lens, the focal level for the silicon beneath the particles was at a higher position than the focal spot. It affects the Raman shift and FWHM of silicon.

The temperatures rises deduced from the FWHM broadening (ΔT) are shown in Figure 4(d). The difference between the two temperature rises ΔT and ΔT_ω (based on Raman shift decrease) is mainly due to the stress inside the silicon wafer around the laser-heated spot. ΔT indicates the real temperature rise inside silicon, and (ΔT - ΔT_ω) indicates a Raman frequency change $\Delta\omega$ derived from the local stress (σ) inside silicon, see Figure 4(e). The high stress inside the silicon under the particle is due to the extremely small laser spot, the high temperature gradient, and focal level effect on the Raman spectra.

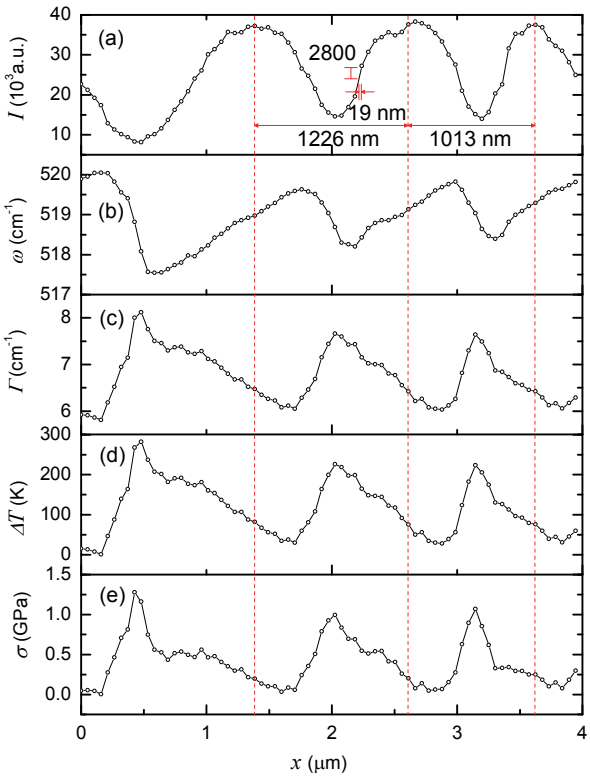

Figure 4. The (a) Raman intensity, (b) frequency, (c) FWHM, (d) temperature rise, and (e) thermal stress inside silicon under particles of 1210 nm diameter with laser irradiation along the x direction.

To explore the particle diameter limit of the far-field nanoscale imaging, 800, 400, and 200 nm particles are used in the experiments. Figure 5 (a) shows large areas of 200 nm monolayer particles on silicon. The average diameter of the particles shown in the SEM image is about 160 nm. The nanoscale imaging experiment is conducted along the x direction within a travel range of 500 nm with a step of 27 nm. The travel range covers about 3 particles. The laser energy flux is 4.7×10^9 W/m^2. The variation of the Raman intensity with x is shown in Figure 5(b). The two distances between the highest intensities are both 160 nm, which agree with the particle diameter. I_{max} is about 3.64×10^4 with a I_{max}/I_{min} of about 1.08 for the first period. The intensity change is about 1400 in a quarter of a period, which is of 40 nm distance, and the intensity ratio is about 1.04.

The relationship between the maximum intensity ratio I_{max}/I_{min} and the particle diameter is shown in Figure 5(c). The I_{max}/I_{min} drops exponentially with the decrease of particle size. As the particle size decreases from 1120 to 160 nm, I_{max}/I_{min} reduces from about 4.8 to 1.1. With the decreasing trend, when the diameter of particles drops to 140 nm, it would be hard to tell the intensity difference within a period. The resolution improves with the increase of the particle size. The ratios are approximately the same for the same particle size with different laser energy fluxes, which indicates that the imaging resolution has little relationship with the energy flux. Figure 5(d) shows the relation between maximum Raman intensity of silicon and the energy flux of incident laser. I_{max} increases linearly with the incident laser energy flux.

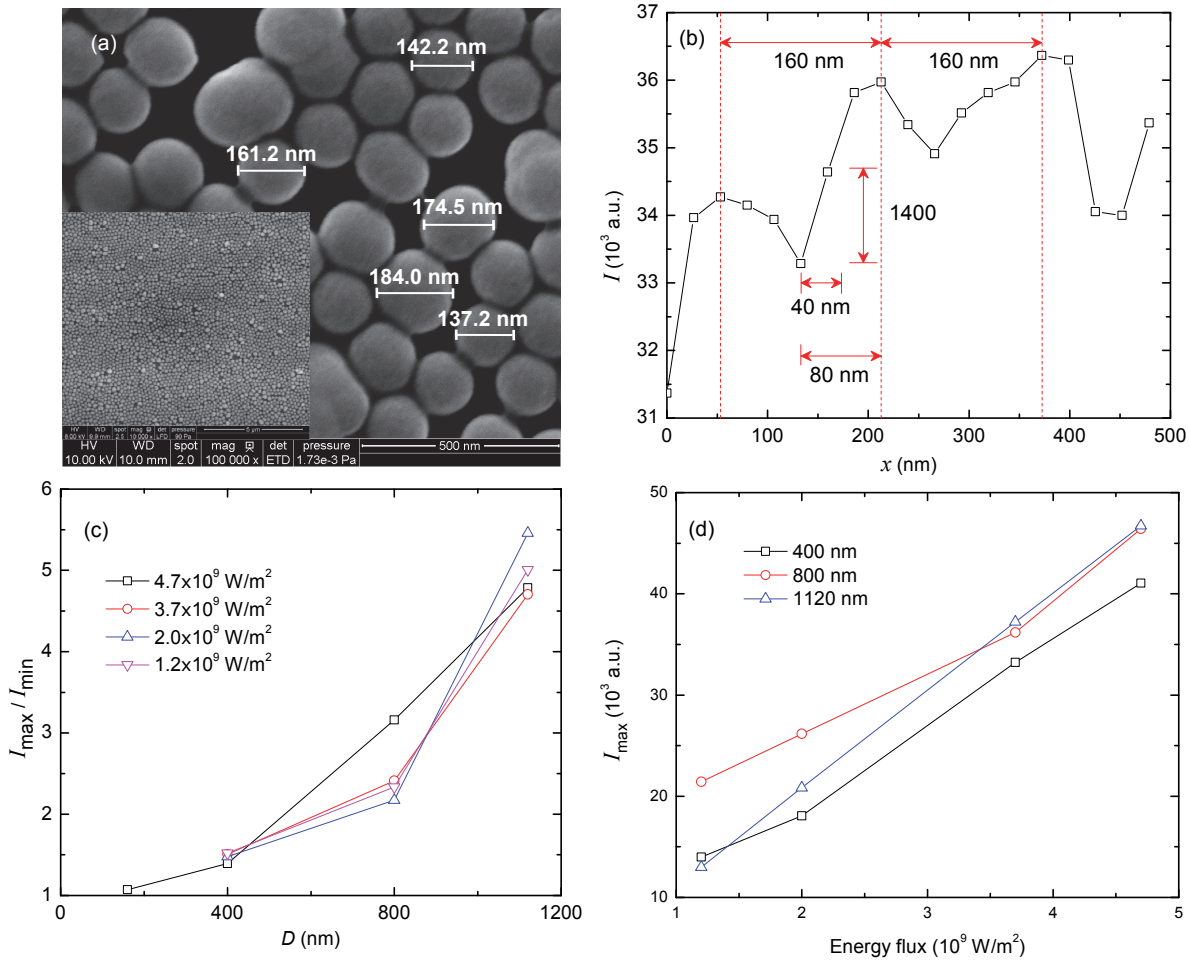

Figure 5. (a) SEM images of 200 nm particles on the substrates. The average diameter of the particles shown in the SEM images is about 160 nm. (b) The Raman intensity of silicon under particles of 200 nm diameter along the x direction. (c) The intensity ratio changes with particle size. (d) The maximum Raman intensity of silicon varies with the laser energy flux.

Physics behind Far-field Nanoscale Imaging

In order to study the mechanism of the temperature and stress rise in the particle-substrate system, electromagnetic simulation is conducted using the high frequency structure simulator (HFSS V14, Ansys, Inc.). The simulation is performed on a platform consisting of a 3.72 GHz AMD ×6 processor and 16 GB RAM. Only the 1210-nm-particle case is studied. Other cases can be treated similarly. A group of models are employed in the simulation with the movement of particles relative to the laser along the x direction. The computational models with dimensions of 1800 nm × 900 nm × 3110 nm consist of about part of five silica particles on a silicon substrate. In consideration of the amount of calculation and mesh density for HFSS, the model is set to be symmetrical in the electric direction. Perfect H symmetry boundary is adopted at the symmetrical plane. Absorbing (radiation) boundaries are applied for other boundary planes in the domain. A plane wave with a wavelength of $\lambda = 532$ nm is incident normally from the top. The wave irradiates the particles and silicon only through an area of 1 × 1 μm^2. Other areas are light shaded with a user defined light-absorbing material. The electric field amplitude of the incident wave is set to 1 V/m. Therefore, the near-field enhancement value, the ratio of scattered to incident electric field amplitude, is the same as the electric field amplitude of the scattered light. At 532 nm, the dielectric permittivities of silica and silicon are $\varepsilon = 2.13 + 0i$ and $\varepsilon = 17.22 + 0.428i$, respectively. The electric conductivities of silica and silicon are 0 and 1.34 × 10^5 S/m, respectively. The relative permittivity, permeability and conductivity of the light-absorbing material are set at -1.79 × 10^{15}, 1.79 × 10^{15} and 0, respectively. Figure 6 shows the electric field distributions inside the substrate-particle system at three typical laser irradiation positions. The maximum electric field varies from 0.8 - 1.1 V/m inside the silicon substrate and from 1.8 - 3.3 V/m inside the substrate-particle system. The laser is focused inside the silicon substrate by the particles mainly within a small zone right beneath each particle that is under laser irradiation.

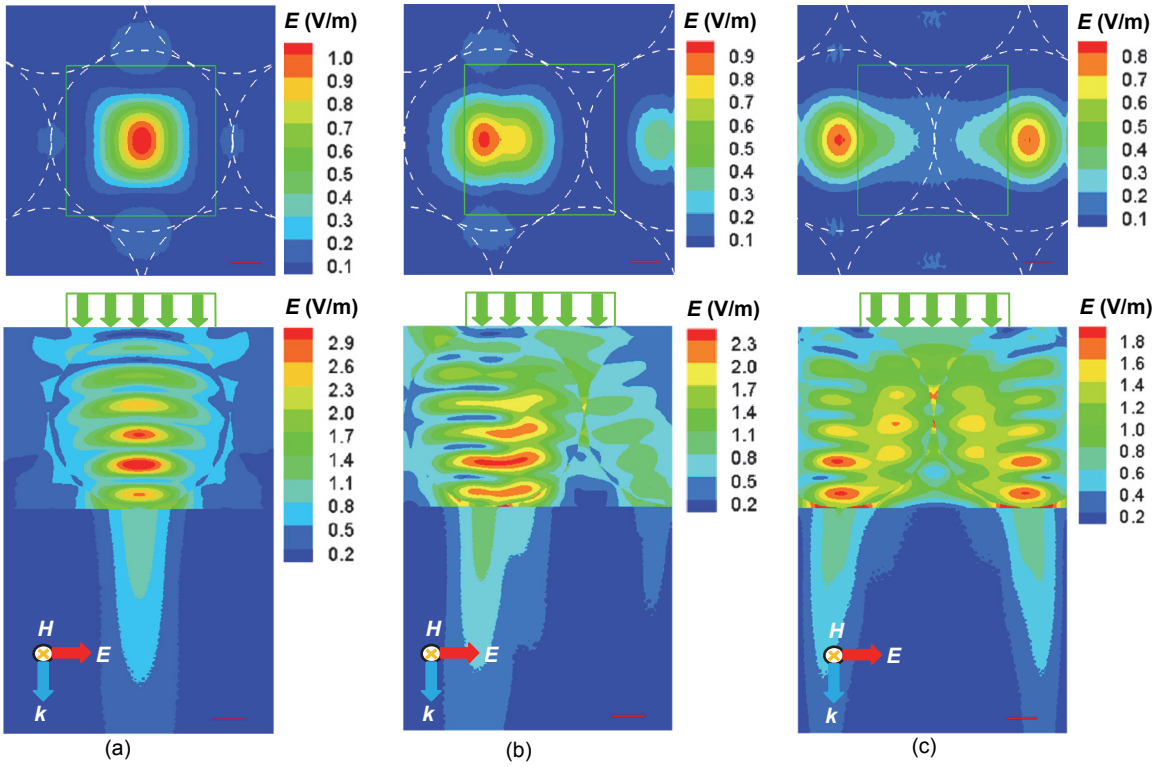

Figure 6. Electric field distributions inside the substrates and particles of 1210 nm diameter at three typical positions in the x direction. The upper figures are top view of the substrates beneath the particles, and the lower figures are central cross-section view of the particles and substrates. The green squares indicate the incident wave region, and the white dashed circles represent the positions of silica particles. The amplitude of electric field is equal to the enhancement factor.

The light intensity ratio between the maximum and minimum values at different positions in simulation is only 1.77, smaller than the Raman intensity ratio in experiments (4.78). There are three main factors considered leading to the difference. The first factor is the relationship between the collected Raman signal and the distance between the objective lens and the focusing point. The collected Raman signal is the strongest when the focusing point inside silicon is at the centre of the objective lens. The signal decreases with the increase of the distance between focusing location and lens. Moreover, Raman intensity of silicon varies with focal level in the vertical direction. The Raman intensity reaches maximum at the focal spot, and decreases with the distance between the sample and laser focal spot position. Finally, the Raman intensity reduces with the increase of the temperature. This is because high temperature caused by particle induced heating changes the band structure in silicon, which restricts the photon interactions necessary to generate Raman signals. The state density and energy of phonons increase as temperature rises, leading to a reduction of Raman intensity.

Conclusions

By employing silica particles as far-field superlenses, we have demonstrated the first combined periodical thermal, stress and structure imaging with lateral resolution beyond the diffraction limit. The resolution is limited in principle by the diameter of the particles, not the illustration wavelength, and the increase of the particle size improves the imaging resolution. Our results indicate that the temperature and stress distribution vary with the periodical surface structure inside a substrate-particle system corresponding to an imaging resolution of 20 nm. The estimated minimum diameter of the particle capable of imaging the structure difference is 140 nm. The experimental results are supported by electromagnetic simulation with finite element analysis. Due to the nanoscale imaging capability and visible frequency operation, the far-field superlens imaging has potential applications in optical metrology, nanolithography and nanotexturing.

Acknowledgements

Support of this work by the National Science Foundation (CMMI-0926704 and CBET-0932573) is gratefully acknowledged.

References

[1] Frey, H.G., Keilmann, F., Kriele, A. & Guckenberger, R. (2002) Enhancing the resolution of scanning near-field optical microscopy by a metal tip grown on an aperture probe, Applied Physics Letters 26, 5030-5032.

[2] Rust, M.J., Bates, M. & Zhuang, X.W. (2006) Sub-diffraction-limit imaging by stochastic optical reconstruction microscopy (STORM), Nature Methods 10, 793-795.

[3] Wang, Z.B., Guo, W., Li, L., Luk'yanchuk, B., Khan, A., Liu, Z., Chen, Z.C. & Hong, M.H. (2011) Optical virtual imaging at 50 nm lateral resolution with a white-light nanoscopes, Nature Communications 2, 218.

[4] Shi, L., Plyasunov, S., Bachtold, A., McEuen, P.L. & Majumdar, A. (2000) Scanning thermal microscopy of carbon nanotubes using batch-fabricated probes, Applied Physics Letters 26, 4295-4297.

[5] McLeod, E. & Arnold, C.B. (2008) Subwavelength direct-write nanopatterning using optically trapped microspheres, Nature Nanotechnology 7, 413-417.

[6] Huang, S.M., Hong, M.H., Luk'yanchuk, B.S., Zheng, Y.W., Song, W.D., Lu, Y.F. & Chong, T.C. (2002) Pulsed laser-assisted surface structuring with optical near-field enhanced effects, Journal of Applied Physics 5, 2495-2500.

[7] Ng, V., Lee, Y.V., Chen, B.T. & Adeyeye, A.O. (2002) Nanostructure array fabrication with temperature-controlled self-assembly techniques, Nanotechnology 13, 554-558.

[8] Balkanski, M., Wallis, R. & Haro, E. (1983) Anharmonic effects in light scattering due to optical phonons in silicon, Physical Review B 4, 1928-1934.

[9] Beechem, T., Graham, S., Kearney, S.P., Phinney, L.M. & Serrano, J.R. (2007) Invited article: simultaneous mapping of temperature and stress in microdevices using micro-Raman spectroscopy, Review of Scientific Instruments 78, 061301.

[10] Bauer, M., Gigler, A.M., Richter, C. & Stark, R.W. (2008) Visualizing stress in silicon micro cantilevers using scanning confocal Raman spectroscopy, Microelectronic Engineering 85, 1443-1446.

[11] Senez, V., Armigliato, A., De Wolf, I., Carnevale, G., Balboni, R., Frabboni, S. & Benedetti, A. (2003) Strain determination in silicon microstructures by combined convergent beam electron diffraction, process simulation, and micro-Raman spectroscopy, Journal of Applied Physics 9, 5574-5583.